γp and $\gamma\gamma$ Physics at High Energies

Torbjörn Sjöstrand[1]

Theory Division, CERN
CH-1211 Geneva 23, Switzerland

ABSTRACT

A real photon has a complicated nature, whereby it may remain unresolved or fluctuate into a vector meson or a perturbative $q\overline{q}$ pair. This implies a model for γp events based on the presence of three main event classes: direct, VMD and anomalous. In $\gamma\gamma$ events, a natural generalization gives three-by-three combinations of the nature of the two incoming photons, and thus six distinct event classes. The properties of these classes are constrained by the choices already made, in the γp model, of cut-off procedures and other aspects. The predicted total $\gamma\gamma$ cross section is in agreement with data and with a simple factorized ansatz with a pomeron and a reggeon term. Event properties undergo a logical evolution from pp to γp to $\gamma\gamma$ events, with larger charged multiplicity, more transverse energy flow and a higher jet rate in the latter process.

1. Introduction

In this talk I report on work carried out in collaboration with Gerhard Schuler. Some of it is already published [1, 2], or has previously appeared in workshop presentations [3].

The study of $\gamma\gamma$ physics has a long history, and it is not our intention here to give a complete list of references. Many topics have been covered by the contributions to recent workshops [4]. For the approach we are going to take, one important line of work is the subdivision of photon interactions by the nature of the photon [5]. Minijet phenomenology has attracted much attention in recent years [6].

However, none of these approaches attempts to give a complete description of γp and $\gamma\gamma$ cross sections and event properties, but only concentrate on specific topics. Here we will try to be more ambitious, and really provide all the necessary aspects in one single framework.

[1] on leave of absence from Department of theoretical physics 2, University of Lund, Lund, Sweden

One main area is still left out of our description: in all that follows, incoming photons are assumed to be on the mass shell. Further issues need to be addressed when photons are virtual. For reasons of clarity, we also restrict ourselves to discussing what happens in the collision between two particles of given momenta. The addition of photon flux factors will complicate the picture, but not add anything fundamentally new.

The reasons for a study of this kind are several. On the one hand, the nature of the real photon is surprisingly complex and still not yet fully understood. On the other hand, the γp cross section at HERA and the $\gamma\gamma$ one at LEP 2 are very large and therefore such events provide a main source of background to other processes. However, at a meeting on multiparticle dynamics, the main reason would be that γp and $\gamma\gamma$ events offers the ultimate challenge (heavy-ion physics aside) of minimum-bias physics: since the photon has a hadronic component, all of hadronic physics is contained in the rich set of processes allowed in interactions involving real photons.

2. Event Classes

To first approximation, the photon is a point-like particle. However, quantum mechanically, it may fluctuate into a (charged) fermion–antifermion pair. The fluctuations $\gamma \leftrightarrow \mathrm{q\overline{q}}$ are of special interest to us, since such fluctuations can interact strongly and therefore turn out to be responsible for the major part of the γp and $\gamma\gamma$ total cross sections, as we shall see. On the other hand, the fluctuations into a lepton pair are uninteresting, since such states do not undergo strong interactions to leading order, and therefore contribute negligibly to total hadronic cross sections. The leptonic fluctuations are perturbatively calculable, with an infrared cut-off provided by the lepton mass itself. Not so for quark pairs, where low-virtuality fluctuations enter a domain of non-perturbative QCD physics. It is therefore customary to split the spectrum of fluctuations into a low-virtuality and a high-virtuality part. The former part can be approximated by a sum over low-mass vector-meson states, customarily (but not necessarily) restricted to the lowest-lying vector multiplet. Phenomenologically, this Vector Meson Dominance (VMD) ansatz turns out to be very successful in describing a host of data. The high-virtuality part, on the other hand, should be in a perturbatively calculable domain.

In total, the photon wave function can then be written as

$$|\gamma\rangle = c_{\mathrm{bare}}|\gamma_{\mathrm{bare}}\rangle + \sum_{V=\rho^0,\omega,\phi,\mathrm{J}/\psi} c_V|V\rangle + \sum_{\mathrm{q=u,d,s,c,b}} c_{\mathrm{q}}|\mathrm{q\overline{q}}\rangle + \sum_{\ell=\mathrm{e},\mu,\tau} c_\ell|\ell^+\ell^-\rangle \qquad (1)$$

(neglecting the small contribution from Υ). In general, the coefficients c_i depend on the scale μ used to probe the photon. Thus $c_\ell^2 \approx (\alpha_{\mathrm{em}}/2\pi)(2/3)\ln(\mu^2/m_\ell^2)$. Introducing a cut-off parameter k_0 to separate the low- and high-virtuality parts of the $\mathrm{q\overline{q}}$ fluctuations, one similarly obtains $c_{\mathrm{q}}^2 \approx (\alpha_{\mathrm{em}}/2\pi)2e_{\mathrm{q}}^2\ln(\mu^2/k_0^2)$. The VMD part corresponds to the range of $\mathrm{q\overline{q}}$ fluctuations below k_0 and is thus μ-independent (assuming

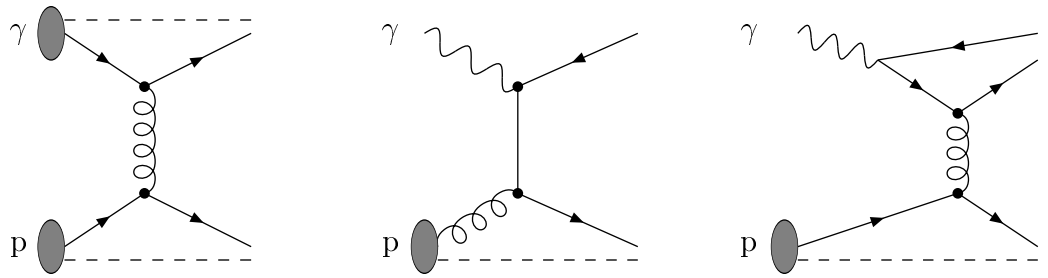

Figure 1: Contributions to hard γp interactions: a) VMD, b) direct, and c) anomalous. Only the basic graphs are illustrated; additional partonic activity is allowed in all three processes. The presence of spectator jets has been indicated by dashed lines, while full lines show partons that (may) give rise to high-$p_\perp$ jets.

$\mu > k_0$). In conventional notation $c_V^2 = 4\pi\alpha_{\rm em}/f_V^2$, with $f_V^2/4\pi$ determined from data to be 2.20 for ρ^0, 23.6 for ω, 18.4 for ϕ and 11.5 for J/ψ [7]. Finally, $c_{\rm bare}$ is given by unitarity: $c_{\rm bare}^2 \equiv Z_3 = 1 - \sum c_V^2 - \sum c_{\rm q}^2 - \sum c_\ell^2$. In practice, $c_{\rm bare}$ is always close to unity. Usually the probing scale μ is taken to be the transverse momentum of a $2 \to 2$ parton-level process. Our fitted value $k_0 \approx 0.5$ GeV (see below) then sets the minimum transverse momentum of a perturbative branching $\gamma \to {\rm q}\overline{\rm q}$.

The subdivision of the above photon wave function corresponds to the existence of three main event classes in γp events, cf. Fig. 1:

1. The VMD processes, where the photon turns into a vector meson before the interaction, and therefore all processes allowed in hadronic physics may occur. This includes elastic and diffractive scattering as well as low-$p_\perp$ and high-$p_\perp$ non-diffractive events.
2. The direct processes, where a bare photon interacts with a parton from the proton.
3. The anomalous processes, where the photon perturbatively branches into a $\rm q\overline{q}$ pair, and one of these (or a daughter parton thereof) interacts with a parton from the proton.

All three processes are of $O(\alpha_{\rm em})$. However, in the direct contribution the photon structure function is of $O(1)$ and the hard scattering matrix elements of $O(\alpha_{\rm em})$, while the opposite holds for the VMD and the anomalous processes. As we already noted, the $\ell^+\ell^-$ fluctuations are not interesting, and there is thus no class associated with them.

The above subdivision is not unique, or even the conventional one. More common is to lump the jet production processes of VMD and anomalous into a class called resolved photons. The remaining 'soft-VMD' class is then defined as not having any jet production at all, but only consisting of low-$p_\perp$ events. We find such a subdivision

counterproductive, since it is then not possible to think of the VMD class as being a scaled-down version (by a factor c_V^2) of ordinary hadronic processes — remember that normal hadronic collisions *do* contain jets part of the time.

In a complete framework, there would be no sharp borders between the three above classes, but rather fairly smooth transition regions that interpolate between the extreme behaviours. However, at our current level of understanding, we do not know how to do this, and therefore push our ignorance into parameters such as the k_0 scale and the $f_V^2/4\pi$ couplings. From a practical point of view, the sharp borders on the parton level are smeared out by parton showers and hadronization. Any Monte Carlo event sample intended to catch a border region would actually consist of a mixture of the three extreme scenarios, and therefore indeed be intermediate. Towards the end of the talk this issue is discussed further.

The difference between the three classes is easily seen in terms of the beam jet structure. The incoming proton always gives a beam jet containing the partons of the proton that did not interact. On the photon side, the direct processes do not give a beam jet at all, since all the energy of the photon is involved in the hard interaction. The VMD ones (leaving aside the elastic and diffractive subprocesses for the moment) give a beam remnant just like the proton, with a 'primordial $k_\perp$' smearing of typically up to half a GeV. The anomalous processes give a beam remnant produced by the $\gamma \to \mathrm{q\overline{q}}$ branching, with a transverse momentum going from k_0 upwards. Thus the transition from VMD to anomalous should be rather smooth.

A generalization of the above picture to $\gamma\gamma$ events is obtained by noting that each of the two incoming photons is described by a wave function of the type given in eq. (1). In total, there are therefore three times three event classes. By symmetry, the 'off-diagonal' combinations appear pairwise, so the number of distinct classes is only six. These are, cf. Fig. 2:

1. VMD×VMD: both photons turn into hadrons, and the processes are therefore the same as allowed in hadron–hadron collisions.
2. VMD×direct: a bare photon interacts with the partons of the VMD photon.
3. VMD×anomalous: the anomalous photon perturbatively branches into a $\mathrm{q\overline{q}}$ pair, and one of these (or a daughter parton thereof) interacts with a parton from the VMD photon.
4. Direct×direct: the two photons directly give a quark pair, $\gamma\gamma \to \mathrm{q\overline{q}}$. Also lepton pair production is allowed, $\gamma\gamma \to \ell^+\ell^-$, but will not be considered by us.
5. Direct×anomalous: the anomalous photon perturbatively branches into a $\mathrm{q\overline{q}}$ pair, and one of these (or a daughter parton thereof) directly interacts with the other photon.
6. Anomalous×anomalous: both photons perturbatively branch into $\mathrm{q\overline{q}}$ pairs, and subsequently one parton from each photon undergoes a hard interaction.

The first three classes above are pretty much the same as the three classes allowed in γp events, since the interactions of a VMD photon and those of a proton are about the same.

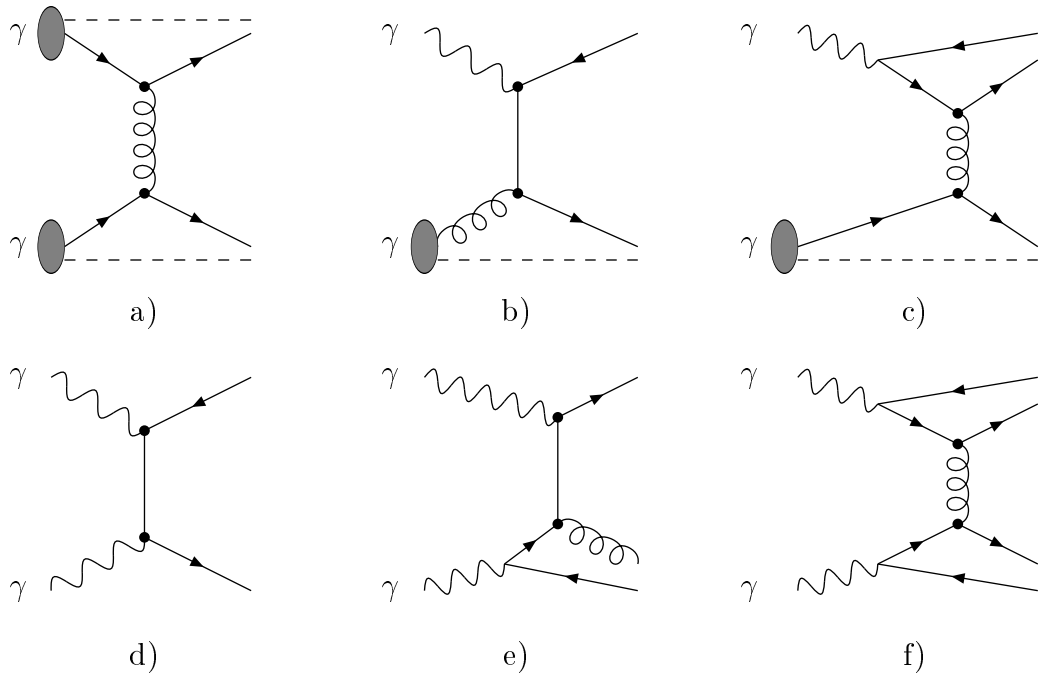

Figure 2: Contributions to hard $\gamma\gamma$ interactions: a) VMD×VMD, b) VMD×direct, c) VMD×anomalous, d) direct×direct, e) direct×anomalous, and f) anomalous×anomalous. Notation as in Fig. 1.

The main parton-level processes that occur in the above classes are:

- The 'direct' processes $\gamma\gamma \to \mathrm{q\overline{q}}$ only occur in class 4.
- The '1-resolved' processes $\gamma\mathrm{q} \to \mathrm{qg}$ and $\gamma\mathrm{g} \to \mathrm{q\overline{q}}$ occur in classes 2 and 5.
- The '2-resolved' processes $\mathrm{qq}' \to \mathrm{qq}'$ (where q′ may also represent an antiquark), $\mathrm{q\overline{q}} \to \mathrm{q'\overline{q}'}$, $\mathrm{q\overline{q}} \to \mathrm{gg}$, $\mathrm{qg} \to \mathrm{qg}$, $\mathrm{gg} \to \mathrm{q\overline{q}}$ and $\mathrm{gg} \to \mathrm{gg}$ occur in classes 1, 3 and 6.
- Elastic, diffractive and low-$p_\perp$ events occur in class 1.

The notation direct, 1-resolved and 2-resolved is the conventional subdivision of $\gamma\gamma$ interactions. The rest is then called 'soft-VMD'. As for the γp case, our subdivision is an attempt to be more precise and internally consistent than the conventional classes allow. One aspect is that we really want to have a VMD×VMD class that is nothing but a scaled-down copy of the $\rho^0\rho^0$ and other vector-meson processes, with a consistent transition between low-$p_\perp$ and high-$p_\perp$ events (see below). Another aspect is that, in a complete description, the VMD and anomalous parts of the photon give rise to different beam remnant structures, as discussed above, even when the hard subprocess itself may be the same.

A third aspect is that our subdivision provides further constraints; these, at least in principle, make the model more predictive. In particular, the parton distributions

of the photon are constrained by the ansatz in eq. (1) to be given by

$$f_a^\gamma(x,\mu^2) = f_a^{\gamma,\mathrm{dir}}(x,\mu^2) + f_a^{\gamma,\mathrm{VMD}}(x,\mu^2) + f_a^{\gamma,\mathrm{anom}}(x,\mu^2;k_0^2) \; . \tag{2}$$

Here

$$f_a^{\gamma,\mathrm{dir}}(x,\mu^2) = Z_3 \, \delta_{a\gamma} \, \delta(1-x) \tag{3}$$

and

$$f_a^{\gamma,\mathrm{VMD}}(x,\mu^2) = \sum_{V=\rho^0,\omega,\phi,\mathrm{J}/\psi} \frac{4\pi\alpha}{f_V^2} f_a^V(x,\mu^2) \; . \tag{4}$$

The anomalous part, finally, is fully calculable perturbatively, given the boundary condition that the distributions should vanish for $\mu^2 = k_0^2$. In principle, everything is therefore given. In practice, the vector-meson distributions are not known, and so one is obliged to make further assumptions, such as $\rho^0 \approx \pi^0 \approx (\pi^+ + \pi^-)/2$. Since the ρ^0 is rather short-lived, it is not impossible that it could be somewhat different from a π, e.g. with fewer partons at small x. A further uncertainty exists in the limit $Q^2 \to 0$, where VMD distributions should vanish; we here use the same approach as introduced for the proton [1]. Overall, a reasonable agreement is obtained with existing deep inelastic scattering data without undue model dependence. By comparison, conventional distributions are defined for resolved processes only:

$$f_a^{\gamma,\mathrm{res}}(x,\mu^2) = f_a^{\gamma,\mathrm{VMD}}(x,\mu^2) + f_a^{\gamma,\mathrm{anom}}(x,\mu^2;k_0^2) \; . \tag{5}$$

The resolved distributions are then assumed to be given in a completely free way, at some input scale, i.e. without any direct relation with the vector-meson distributions.

3. Cross Sections

Total hadronic cross sections show a characteristic fall-off at low energies and a slow rise at higher energies. This behaviour can be parametrized by the form

$$\sigma_{\mathrm{tot}}^{AB}(s) = X^{AB} s^\epsilon + Y^{AB} s^{-\eta} \tag{6}$$

for $A + B \to X$. The powers ϵ and η are universal, with fit values [8]

$$\epsilon \approx 0.0808 \; , \qquad \eta \approx 0.4525 \; , \tag{7}$$

while the coefficients X^{AB} and Y^{AB} are process-dependent. Equation (6) can be interpreted within Regge theory, where the first term corresponds to pomeron exchange and gives the asymptotic rise of the cross section. Ultimately, this increase violates the Froissart–Martin bound [9]; ϵ should therefore be thought of as slowly decreasing with energy (owing to multi-pomeron exchange effects), although data at current energies are well fitted by a constant ϵ. The second term, the reggeon one, is mainly of interest at low energies. For the purpose of our study we do not rely on the Regge interpretation of eq. (6), but can merely consider it as a convenient parametrization.

The VMD part of the γp cross section should have a similar behaviour, but there is no compelling reason why the direct and anomalous parts would have to. However, empirically, the γp data are well described by

$$\sigma_{\rm tot}^{\gamma{\rm p}}(s) \approx 67.7\, s^{\epsilon} + 129\, s^{-\eta} \quad [\mu{\rm b}], \tag{8}$$

with s in GeV^2. (Cross-sections are throughout given in mb for hadron–hadron interactions, in μb for γ–hadron ones and in nb for $\gamma\gamma$ ones.) Actually, the above formula is a prediction [8] preceding the HERA data [10].

If we take the Regge-theory ansatz seriously also for the photon, it is possible to derive an expression for the total $\gamma\gamma$ cross section

$$\sigma_{\rm tot}^{\gamma\gamma}(s) \approx 211\, s^{\epsilon} + 297\, s^{-\eta} \quad [{\rm nb}]. \tag{9}$$

This is based on the assumption that the pomeron and reggeon terms factorize, $X^{AB} = \beta_{A\mathbb{P}}\beta_{B\mathbb{P}}$ and $Y^{AB} = \gamma_{A\mathbb{R}}\gamma_{B\mathbb{R}}$, so that $X^{\gamma\gamma} = (X^{\gamma{\rm p}})^2/X^{\rm pp}$ and $Y^{\gamma\gamma} = (Y^{\gamma{\rm p}})^2/Y^{\rm pp}$, with $X^{\rm pp} \approx 21.70$ and $Y^{\rm pp} \approx 56.08$. In hadronic cross sections, factorization seems valid for the pomeron term but not for the reggeon one, e.g. $X^{\overline{\rm p}{\rm p}} = X^{\rm pp}$ while $Y^{\overline{\rm p}{\rm p}} \approx 98.39 \gg Y^{\rm pp}$. An equally valid guess for $Y^{\gamma\gamma}$ would then be obtained by $Y^{\gamma\gamma} = 2(Y^{\gamma{\rm p}})^2/(Y^{\rm pp}+Y^{\overline{\rm p}{\rm p}}) \approx 215$. The uncertainty in $Y^{\gamma\gamma}$ only affects the low-energy behaviour, and so is not critical for us.

Note that factorization is assumed to hold separately for the pomeron and the reggeon terms, not for the total cross section itself. That is, the relation $\sigma_{\rm tot}^{\gamma\gamma} = (\sigma_{\rm tot}^{\gamma{\rm p}})^2/\sigma_{\rm tot}^{\rm pp}$ is not exact in this approach, although numerically it is a very good approximation.

Our eq. (9) above should be compared with the time-honoured expression $\sigma^{\gamma\gamma} = 240 + 270/W$ [11]. This corresponds to a critical pomeron, $\epsilon = 0$, as was commonly assumed in the early seventies, and an $\eta = 0.5$, but it is otherwise in the same spirit as our formula. Also numerically the two closely agree at not too large energies.

One should remember that our expression (9) is here 'derived' based on a simple Regge-theory ansatz that has no real validity for the photon. Next we will proceed to study the contributions of the individual event classes. The constraints that come from γp physics data then directly feed into constraints on the contribution from these classes and therefore on the total $\gamma\gamma$ cross section. At the end of the day we will therefore show that a cross section behaving roughly like eq. (9) should be a good approximation. In doing so, the properties of the event classes are also fixed, to a large extent.

Based on the subdivision into event classes, the total γp cross section may be written as

$$\sigma_{\rm tot}^{\gamma{\rm p}} = \sigma_{\rm VMD}^{\gamma{\rm p}} + \sigma_{\rm dir}^{\gamma{\rm p}} + \sigma_{\rm anom}^{\gamma{\rm p}} \tag{10}$$

and the total $\gamma\gamma$ one as

$$\sigma_{\rm tot}^{\gamma\gamma} = \sigma_{\rm VMD\times VMD}^{\gamma\gamma} + 2\sigma_{\rm VMD\times dir}^{\gamma\gamma} + 2\sigma_{\rm VMD\times anom}^{\gamma\gamma} + \sigma_{\rm dir\times dir}^{\gamma\gamma} + 2\sigma_{\rm dir\times anom}^{\gamma\gamma} + \sigma_{\rm anom\times anom}^{\gamma\gamma}\ . \tag{11}$$

Here we explicitly keep the factor of 2 for the off-diagonal terms, where the rôle of the two incoming photons may be interchanged.

The Vp cross sections may be parametrized as

$$\sigma_{\mathrm{tot}}^{\rho^0\mathrm{p}} \approx \sigma_{\mathrm{tot}}^{\omega\mathrm{p}} \approx \frac{1}{2}\left(\sigma_{\mathrm{tot}}^{\pi^+\mathrm{p}} + \sigma_{\mathrm{tot}}^{\pi^-\mathrm{p}}\right) \approx 13.63\, s^{\epsilon} + 31.79\, s^{-\eta} \quad [\mathrm{mb}], \tag{12}$$

$$\sigma_{\mathrm{tot}}^{\phi\mathrm{p}} \approx \sigma_{\mathrm{tot}}^{\mathrm{K}^+\mathrm{p}} + \sigma_{\mathrm{tot}}^{\mathrm{K}^-\mathrm{p}} - \sigma_{\mathrm{tot}}^{\pi^-\mathrm{p}} \approx 10.01\, s^{\epsilon} - 1.51\, s^{-\eta} \quad [\mathrm{mb}]. \tag{13}$$

(The J/ψp cross section is taken to be about a tenth of the ϕp one, with a large amount of uncertainty; it is included in the complete analysis but is neglected in our discussion here.) Again using factorization for the pomeron and reggeon terms separately, the total cross section for two vector mesons is

$$\sigma_{\mathrm{tot}}^{V_1V_2} \approx \frac{X^{\mathrm{p}V_1} X^{\mathrm{p}V_2}}{X^{\mathrm{pp}}}\, s^{\epsilon} + \frac{Y^{\mathrm{p}V_1} Y^{\mathrm{p}V_2}}{Y^{\mathrm{pp}}}\, s^{-\eta}\ . \tag{14}$$

For a description of VMD events, a further subdivision into elastic (el), diffractive (sd and dd for single and double diffractive) and non-diffractive (nd) events is required. Keeping only the simplest diffractive topologies, one may write

$$\sigma_{\mathrm{tot}}^{AB}(s) = \sigma_{\mathrm{el}}^{AB}(s) + \sigma_{\mathrm{sd(XB)}}^{AB}(s) + \sigma_{\mathrm{sd(AX)}}^{AB}(s) + \sigma_{\mathrm{dd}}^{AB}(s) + \sigma_{\mathrm{nd}}^{AB}(s)\ . \tag{15}$$

The elastic and diffractive cross sections for all required Vp and V_1V_2 processes have been calculated and parametrized in the context of our model presented in ref. [2]. The non-diffractive cross-section is then given by whatever is left. The σ_{nd} may be further subdivided into a low-$p_\perp$ and a high-$p_\perp$ class. Since the $2 \to 2$ parton–parton scattering cross sections are divergent in the limit $p_\perp \to 0$, some further care is needed for this classification. We expect the perturbative formulae to break down at small $p_\perp$, since an exchanged gluon with a large transverse wavelength $\lambda_\perp \sim 1/p_\perp$ cannot resolve the individual colour charges inside a hadron. The hadron being a net colour singlet, the effective coupling should therefore vanish in this limit. A parameter $p_{\perp\mathrm{min}}$ is introduced to describe the border down to which the perturbative expression is assumed to be valid [1]:

$$p_{\perp\mathrm{min}}(s) = p_{\perp\mathrm{min}}^{\mathrm{VMD}}(s) \approx 1.3 + 0.15\,\frac{\ln(E_{\mathrm{cm}}/200)}{\ln(900/200)} \quad [\mathrm{GeV}]\ . \tag{16}$$

The jet rate above $p_{\perp\mathrm{min}}$ may still be large, in fact even larger than the total σ_{nd}. It is therefore necessary to allow for the possibility of having several perturbative parton–parton interactions in one and the same event, i.e. to unitarize the jet emission probability. We do this using the formalism of ref. [12].

The total VMD cross sections are obtained as weighted sums of the allowed vector-meson states,

$$\sigma_{\mathrm{VMD}}^{\gamma\mathrm{p}} = \sum_V \frac{4\pi\alpha_{\mathrm{em}}}{f_V^2}\,\sigma_{\mathrm{tot}}^{V\mathrm{p}} \approx 53.4\, s^{\epsilon} + 115\, s^{-\eta} \quad [\mu\mathrm{b}], \tag{17}$$

$$\sigma_{\mathrm{VMD}\times\mathrm{VMD}}^{\gamma\gamma} = \sum_{V_1} \frac{4\pi\alpha_{\mathrm{em}}}{f_{V_1}^2} \sum_{V_2} \frac{4\pi\alpha_{\mathrm{em}}}{f_{V_2}^2}\,\sigma_{\mathrm{tot}}^{V_1V_2} \approx 131\, s^{\epsilon} + 236\, s^{-\eta} \quad [\mathrm{nb}]. \tag{18}$$

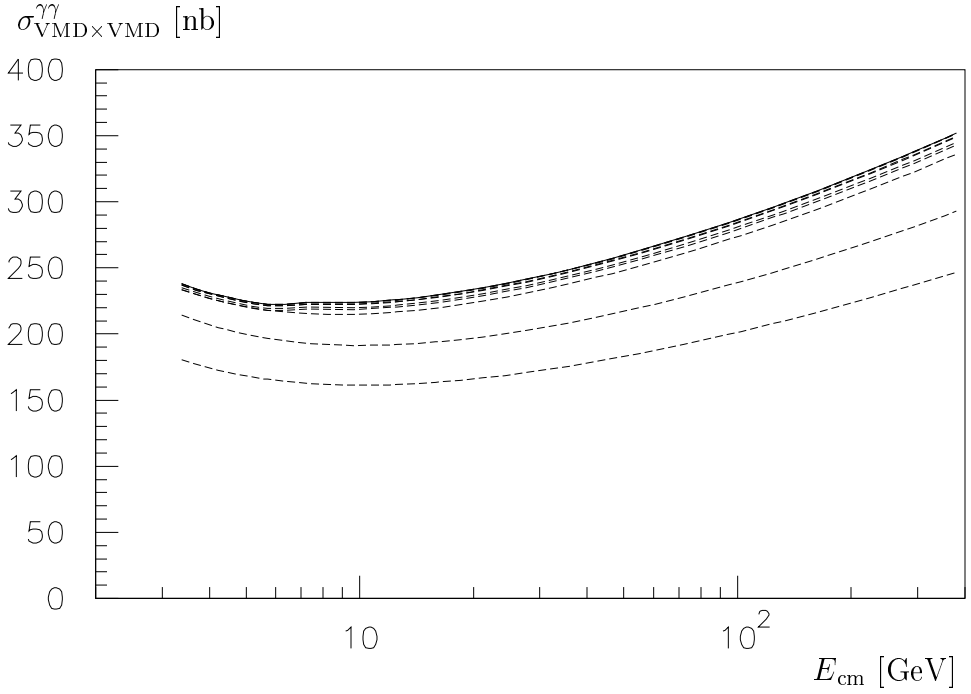

Figure 3: The total VMD×VMD cross section, full curve, and its subdivision by vector-meson combination. The components are separated by dashed curves, from bottom to top: $\rho^0\rho^0$, $\rho^0\omega$, $\rho^0\phi$, $\rho^0\mathrm{J}/\psi$, $\omega\omega$, $\omega\phi$, $\omega\mathrm{J}/\psi$, $\phi\phi$, $\phi\mathrm{J}/\psi$, and $\mathrm{J}/\psi\mathrm{J}/\psi$. Some of the latter components are too small to be resolved in the figure.

In Fig. 3 we show the breakdown of $\sigma^{\gamma\gamma}_{\mathrm{VMD}\times\mathrm{VMD}}$ by vector-meson combination. Obviously the $\rho^0\rho^0$ combination dominates. The same kind of formulae as above also apply for the subdivision into elastic, diffractive and non-diffractive events. This subdivision is shown in Fig. 4 for the sum of all meson combinations, which then mainly reflects the $\rho^0\rho^0$ composition.

Comparing eqs. (8) and (17), about 80% of the γp total cross section is seen to come from the VMD term. The remaining 20% is to be attributed to the direct and anomalous components. At small energies the anomalous part is negligible, and so the dependence of the direct cross section on k_0 can be used to determine this parameter. We obtain a value of $k_0 \approx 0.5$ GeV, which is consistent with the simple-minded answer $k_0 \approx m_\phi/2$, and also gives a reasonable $f_a^{\gamma,\mathrm{res}}(x,\mu^2)$ [1]. The anomalous process contains two cut-off parameters, the k_0 scale for the photon to branch to a perturbative $\mathrm{q\overline{q}}$ pair and a $p_{\perp\mathrm{min}}^{\mathrm{anom}}$ scale for one of the anomalous-photon partons to interact in a hard process. As a first guess, one might choose $p_{\perp\mathrm{min}}^{\mathrm{anom}}$ also to be given by eq. (16). However, this turns out to give a cross section increasing too rapidly.

Physically, it is understandable why hard processes should be more suppressed at small $p_\perp$ in anomalous processes than in VMD ones: the anomalous photon corre-

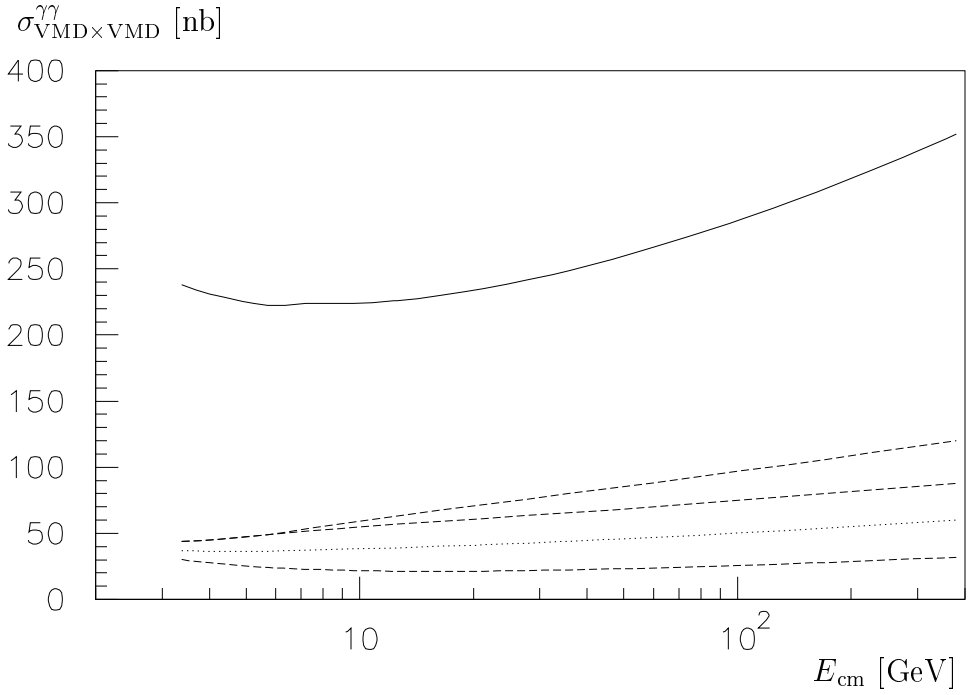

Figure 4: The total VMD×VMD cross section, full curve, and its subdivision by event topology. The components are separated by dashed curves, from bottom to top: elastic, single diffractive (split for the two sides by the dotted curve), double diffractive, and non-diffractive (including jet events unitarized).

sponds to a $q\overline{q}$ pair of larger virtuality than a VMD one, and hence of smaller spatial extent. The best recipe for including this physics aspect is not well understood. Remembering that the anomalous cross section is the product (or, more precisely, the convolution) of the anomalous parton distributions and the hard partonic $2 \to 2$ scattering cross sections, one can, purely pragmatically, imagine two extreme procedures to weaken the too-strong rise of $\sigma^{\gamma p}_{\mathrm{anom}}$: either reduce the partonic cross section by increasing $p^{\mathrm{anom}}_{\perp\mathrm{min}}$, or decrease the values of the anomalous parton distributions by choosing a smaller value for the scale μ, compare eq. (2). Over the HERA energy range, say 100 GeV $\leq E_{\mathrm{cm}} \leq$ 300 GeV, both choices

$$p^{\mathrm{anom}}_{\perp\mathrm{min}}(s) = 1.5 + 0.0035\, E_{\mathrm{cm}} \ \ [\mathrm{GeV}] \qquad ; \qquad \mu = p_\perp \tag{19}$$

$$p^{\mathrm{anom}}_{\perp\mathrm{min}}(s) = \qquad p^{\mathrm{VMD}}_{\perp\mathrm{min}}(s) \qquad ; \qquad \mu = \frac{p_\perp}{r} \quad , \quad r \approx p^{\mathrm{VMD}}_{\perp\mathrm{min}}/k_0 \tag{20}$$

give sensible answers, whereof we will use (19) as our main option. The resulting subdivision of the γp total cross section is shown in Fig. 5. A further alternative will be discussed in section 5.

Turning to the $\gamma\gamma$ cross sections, in principle all free parameters have now been fixed, and the cross section for each of the six event classes can be obtained. The VMD×VMD one has already been discussed; the others are given as integrals of

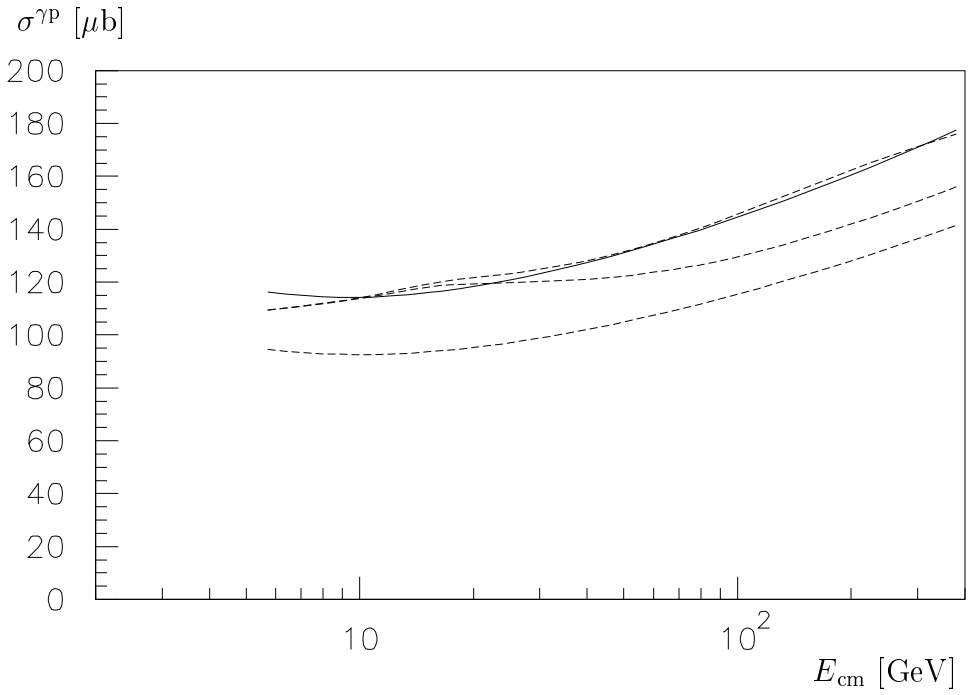

Figure 5: The total γp cross section and its subdivision by event topology. Full curve: the parametrization of eq. (8). The dashed curves, from bottom to top: VMD, VMD+direct and VMD+direct+anomalous.

$2 \to 2$ scattering cross sections above the respective $p_\perp$ cut-offs. When forming the sum, eq. (11), it should be remembered that the first three classes are the dominant ones. In fact, since the direct and anomalous components together give about 20% of the γp total cross section, the expectation is that the last three classes together would only give a 4% contribution to the total $\gamma\gamma$ cross section. Apart from a relatively large uncertainty in the anomalous$\times$anomalous component, this is also the way it works out when doing the integrations. The first three classes, on the other hand, are all related to the respective γp classes, with only a replacement of a p by a V (and an extra weight factor $4\pi\alpha_{\rm em}/f_V^2$). This makes the argumentation for eq. (9) credible, in spite of the absense of a (well-defined) coupling between a direct photon and a pomeron.

The $\sigma_{\rm tot}^{\gamma\gamma}$ obtained by integration of the six components is compared with eq. (9) and experimental data in Fig. 6. As already discussed, the results of the integration are uncertain by some amount, so within this band of uncertainty the agreement with eq. (9) is very good. It is also readily seen that data are not (yet) precise enough to provide any real constraints, but are in generally good agreement with both approaches.

One can also compare our $\sigma_{\rm tot}^{\gamma\gamma}$ with the numbers obtained in various minijet-based approaches [6]. For $E_{\rm cm} = 200$ GeV, cross sections in the range 1000–1800 nb

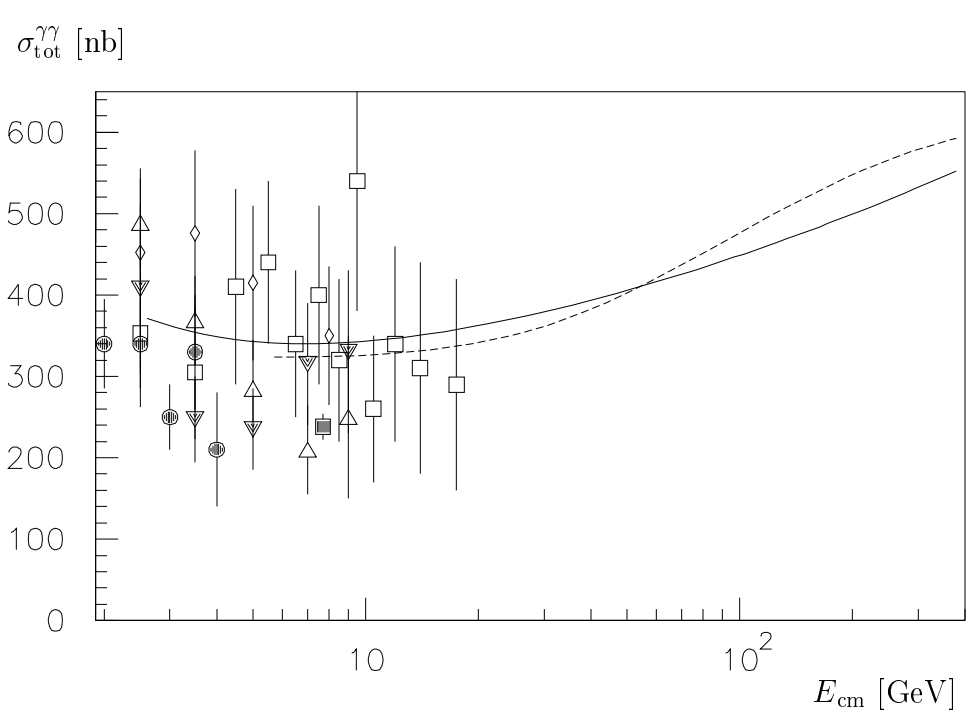

Figure 6: The total $\gamma\gamma$ cross section. Full curve: the parametrization of eq. (9). Dashed curve: result from sum of integrations of the six components. Data points: open triangles PLUTO 1984, filled triangles PLUTO 1986, squares TPC/2γ 1985, spades TPC/2γ 1991, circles MD-1 1991, full square CELLO 1991 [13].

are typically obtained, but are reduced to about 500 nb if unitarity is enforced, in agreement with our results.

4. Event Properties

The subdivision of the total γp and $\gamma\gamma$ cross sections above, with the related choices of cut-off parameters etc., specifies the event composition at the hard-scattering level. For studies of the complete event structure, it is necessary to add models for initial- and final-state QCD radiation (parton showers), for beam remnants, and for fragmentation and secondary decays [1]. A Monte Carlo generation of complete hadronic final states is obtained with PYTHIA/JETSET [14]. Thus any experimental quantity can be studied. This section gives some representative examples. In particular, we compare the properties of pp, γp and $\gamma\gamma$ events. It should be noted that pp and $\overline{\rm p}$p events are very similar for the quantities studied here. Unless otherwise specified, the figures refer to an $E_{\rm cm} = \sqrt{s_{\gamma\gamma}} = 100$ GeV. As we will show at the end of the section, the qualitative features do not depend critically on this choice.

The total summed transverse energy per event is shown in Fig. 7. One observes a steady progression, with $\langle \sum E_\perp \rangle_{\rm pp} < \langle \sum E_\perp \rangle_{\gamma{\rm p}} < \langle \sum E_\perp \rangle_{\gamma\gamma}$. This pattern, of more

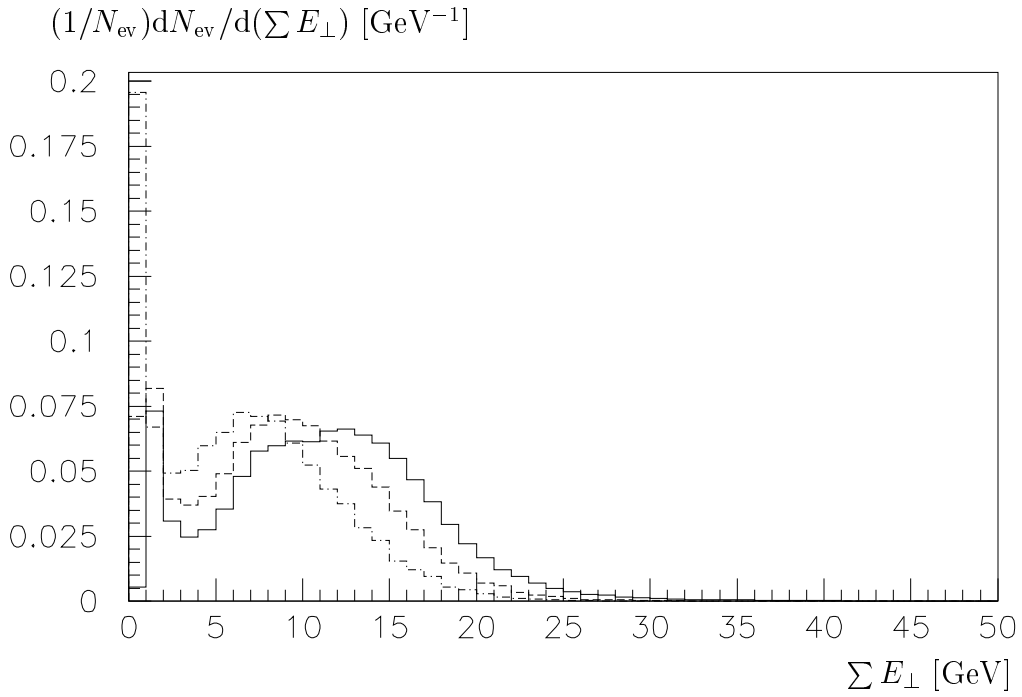

Figure 7: The total transverse energy per event for different beams: $\gamma\gamma$: full histogram; γp: dashed one: and pp: dash-dotted one.

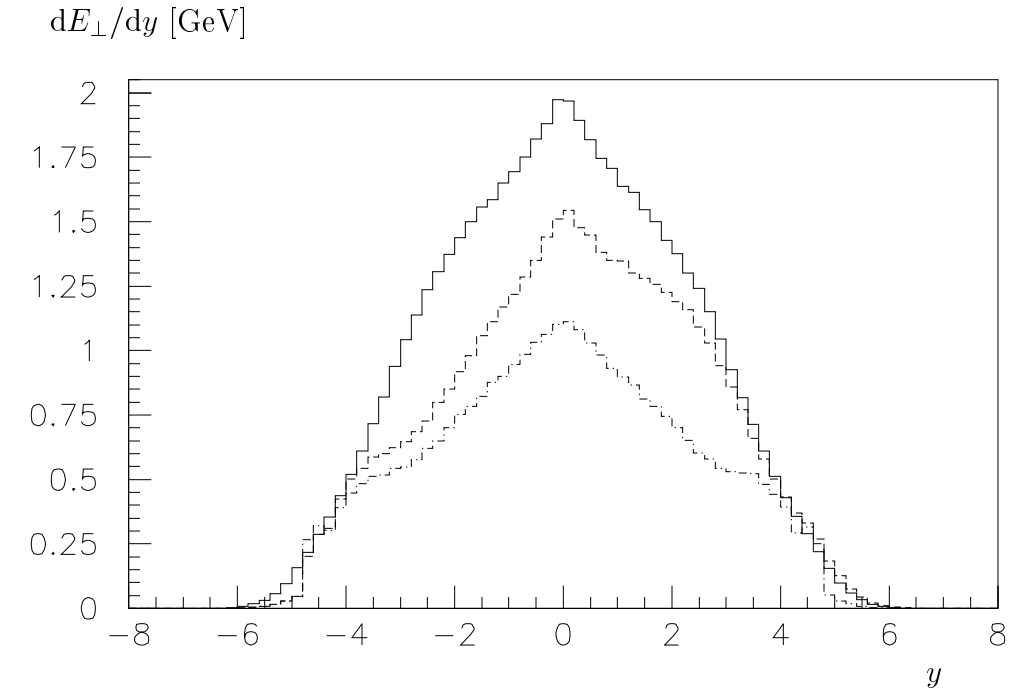

Figure 8: Transverse energy flow as a function of rapidity for different beams: $\gamma\gamma$: full histogram; γp: dashed one; and pp: dash-dotted one.

activity for a γ than for a p, is seen in essentially all distributions. It is mainly related with the large activity expected for interactions involving the anomalous photon component, because of the larger $p_{\perp\min}^{\mathrm{anom}}$. The tail out to very large $\sum E_\perp$ is dominated by the direct processes, in part because of the absence of structure functions. The spike at small $\sum E_\perp$ is due to elastic events, i.e. $\mathrm{pp} \to \mathrm{pp}$, $\gamma\mathrm{p} \to \rho^0\mathrm{p}$, $\gamma\gamma \to \rho^0\rho^0$, or the like. This spike is less pronounced for $\gamma\gamma$, due to three factors: the VMD$\times$VMD component is only a part of the $\gamma\gamma$ cross section, elastic scattering is a smaller fraction of the total $\rho^0\rho^0$ cross section than it is for pp, and kinetic energy in the $\rho^0 \to \pi^+\pi^-$ decays add to the total transverse energy.

The $E_\perp$ flow as a function of rapidity, $\mathrm{d}E_\perp/\mathrm{d}y$, is given in Fig. 8. It illustrates how γp interpolates between pp and $\gamma\gamma$: around the direction of the incoming photon, the γp events look like the $\gamma\gamma$ ones, while they look more like pp ones in the opposite direction, with an intermediate behaviour in the central region.

The charged-multiplicity distributions follow essentially the same pattern as shown for the $\sum E_\perp$ ones in Figs. 7 and 8, and are therefore not included here. There is one noteworthy exception, however: the direct$\times$direct component does not have a tail out to large multiplicities. That is, even if the process $\gamma\gamma \to \mathrm{q\overline{q}}$ can generate large $p_\perp$ values, the absence of any beam jets keeps the multiplicity down.

The transverse momentum spectrum of charged particles is shown in Fig. 9. The larger high-$p_\perp$ tail of the $\gamma\gamma$ processes is one of the simplest observables to experimentally establish differences between pp, γp and $\gamma\gamma$. Of course, the cause of the differences is to be sought in the higher jet rates associated with photon interactions. The jet spectra are compared in Fig. 10, using a simple cone algorithm where a minimum $E_\perp$ of 5 GeV is required inside a cone of $\Delta R = \sqrt{(\Delta\eta)^2 + (\Delta\phi)^2} < 1$. Already for an $E_{\perp\mathrm{jet}}$ of 5 GeV there are about ten times as many jets in $\gamma\gamma$ as in pp, and this ratio then increases with increasing $E_{\perp\mathrm{jet}}$.

To illustrate the energy dependence of these distributions, Figs. 11 and 12 give the $\mathrm{d}E_\perp/\mathrm{d}y$ flow for $\gamma\gamma$ c.m. energies of 25 and 400 GeV, respectively. These can be compared with the result for 100 GeV in Fig. 8. Qualitatively, the same pattern is seen at all three energies, although relative differences tend to be somewhat reduced at larger energies. This is also true for other observables, such as jet rates. One reason is that the possibility of multiple parton–parton interactions in the VMD component pushes up the activity in those events at larger energies, and thus brings them closer to the anomalous class. The importance of the direct class, on the other hand, is reduced at large energies. Further, at large energies, jet production is dominantly initiated by small-x incoming partons, where the VMD and anomalous distributions are more similar than at large x (although still different).

5. The VMD/Direct/Anomalous Interface

In the γp description, the VMD, direct and anomalous classes have so far been considered separately. The complete physics picture presumably would provide smooth

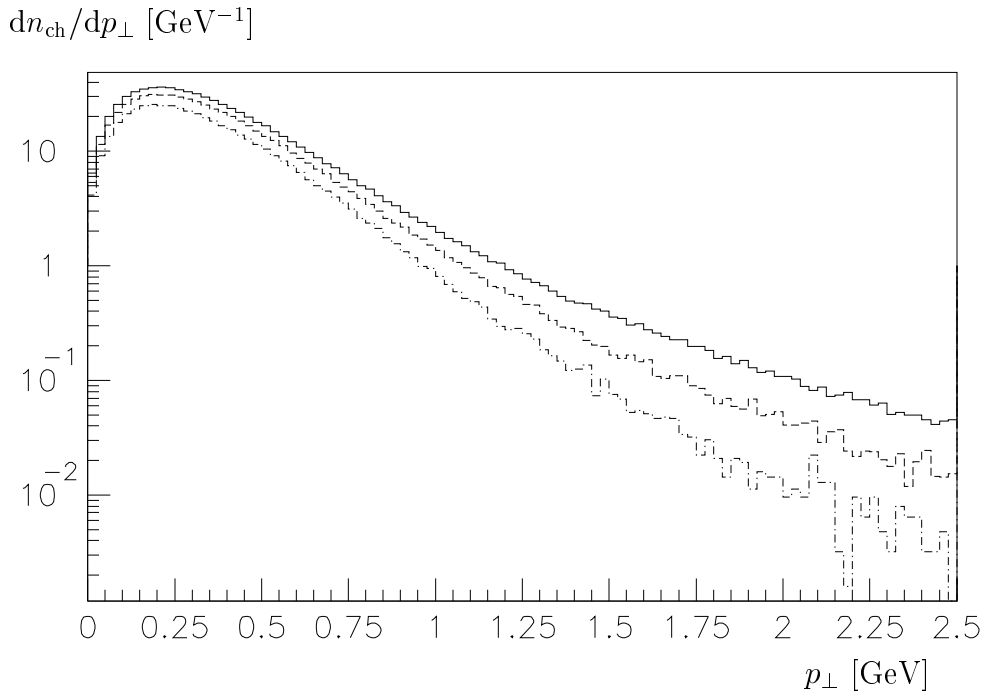

Figure 9: Charged particle inclusive $p_\perp$ spectra for different beams: $\gamma\gamma$: full histogram; γp: dashed one; and pp: dash-dotted one.

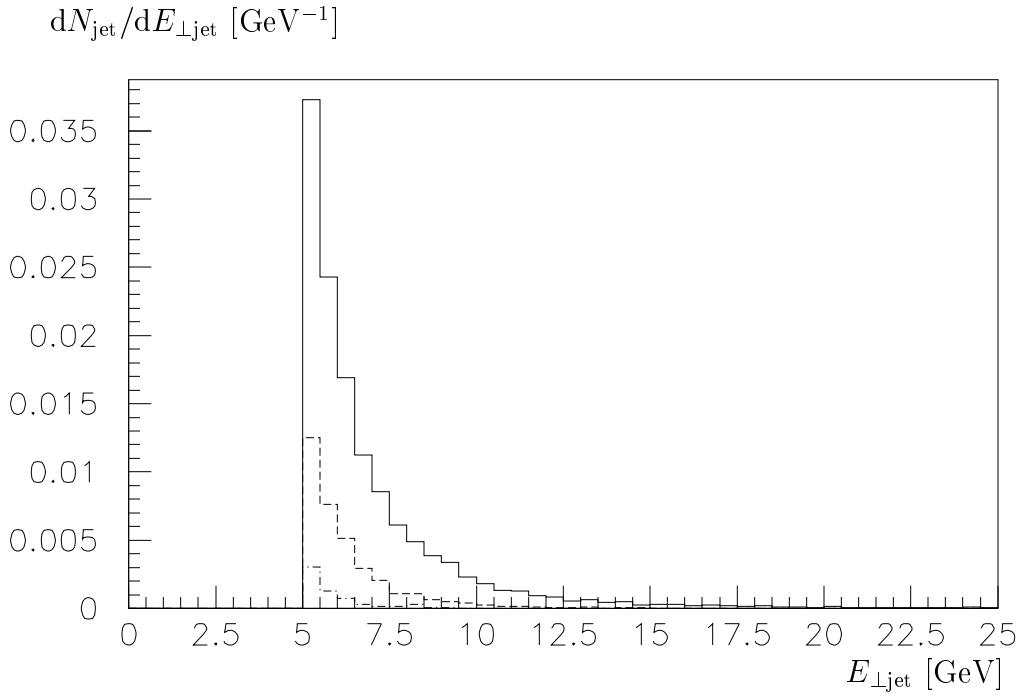

Figure 10: Jet rate as function of the transverse jet energy for different beams: $\gamma\gamma$: full histogram; γp: dashed one; and pp: dash-dotted one.

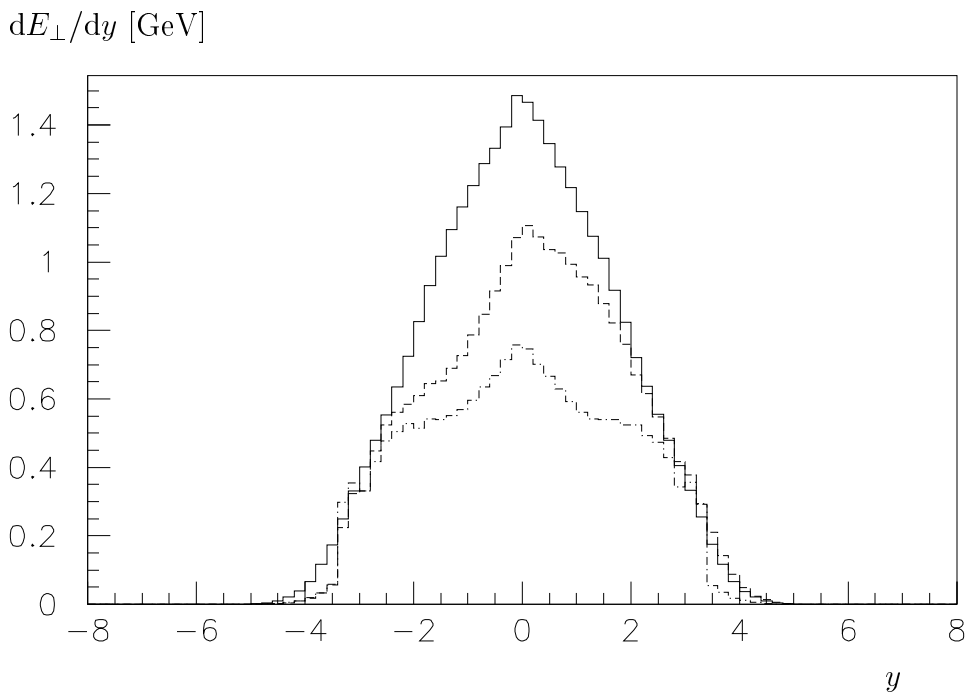

Figure 11: Transverse energy flow for $E_{\rm cm} = 25$ GeV as a function of rapidity for different beams: $\gamma\gamma$: full histogram; γp: dashed one; and pp: dash-dotted one.

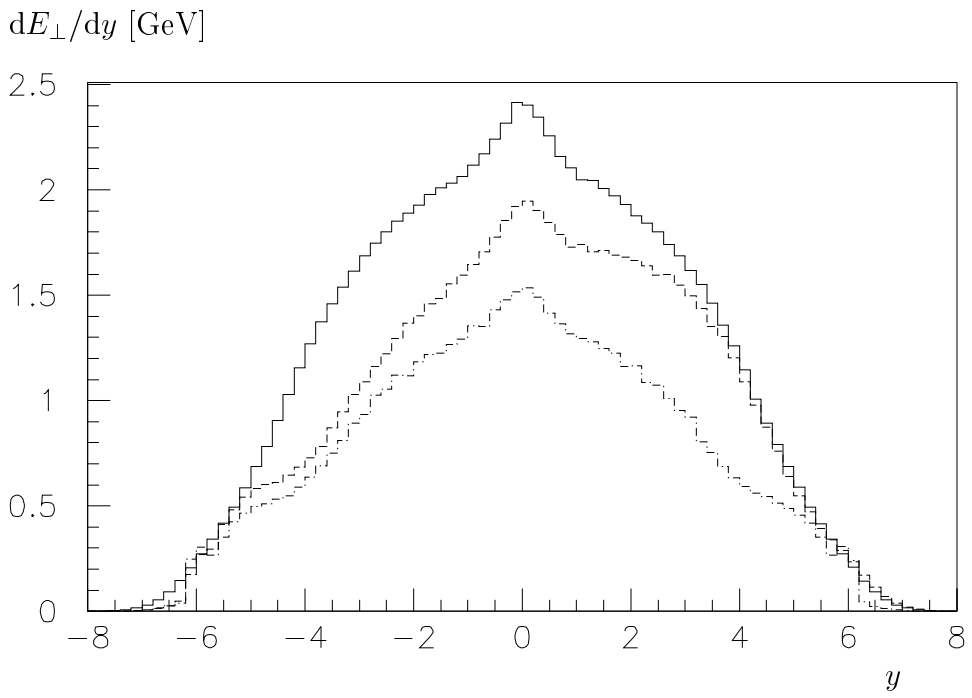

Figure 12: Transverse energy flow for $E_{\rm cm} = 400$ GeV as a function of rapidity. Notation as in Fig. 11.

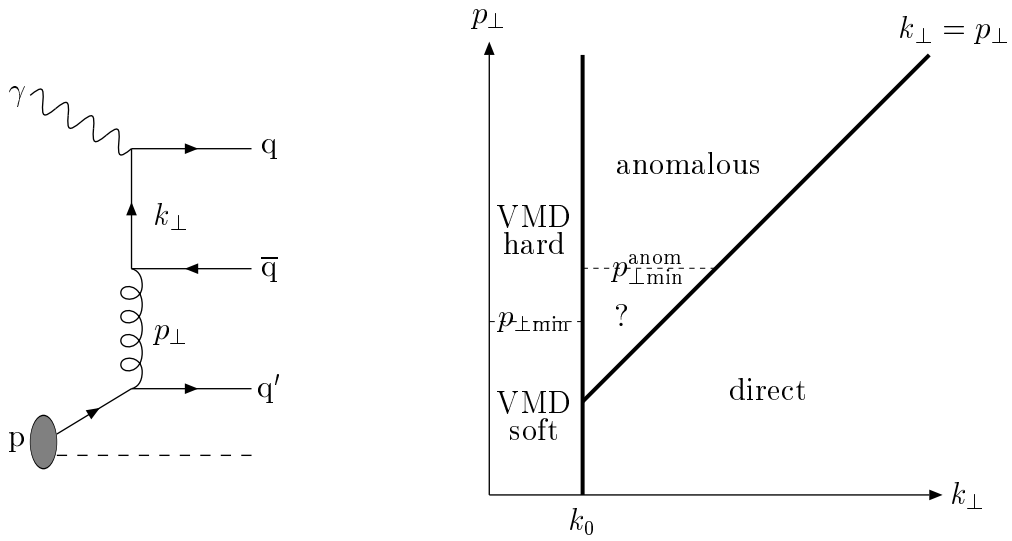

Figure 13: (a) Schematic graph for a hard γp process, illustrating the concept of two different scales. (b) The allowed phase space for this process, with the subdivision into event classes.

transitions between the various possibilities. We are in the process of studying this aspect, and present here a few preliminary results. Once γp is understood, the extension of these ideas to $\gamma\gamma$ should be straightforward.

Consider the simple graph of Fig. 13a. There are two transverse momentum scales, $k_\perp$ and $p_\perp$. Here $k_\perp$ is related to the $\gamma \to \mathrm{q\overline{q}}$ vertex while $p_\perp$ is the hardest QCD $2 \to 2$ subprocess of the ladder between the photon and the proton. (Further softer ladders are omitted for clarity.) The allowed phase space can then conveniently be represented by a two-dimensional plane, Fig. 13b. The region $k_\perp < k_0$ corresponds to a small transverse momentum at the $\gamma \to \mathrm{q\overline{q}}$ vertex, and thus to VMD processes. For $k_\perp > k_0$, the events are split along the diagonal $k_\perp = p_\perp$. If $k_\perp > p_\perp$, the hard $2 \to 2$ process of Fig. 13a is $\gamma\mathrm{g} \to \mathrm{q\overline{q}}$, and the lower part of the graph is part of the leading log QCD evolution of the gluon distribution inside the proton. These events are direct ones. If $p_\perp > k_\perp$, on the other hand, the hard process is $\overline{\mathrm{q}}\mathrm{q}' \to \overline{\mathrm{q}}\mathrm{q}'$, and the $\gamma \to \mathrm{q\overline{q}}$ vertex builds up the quark distribution inside a photon. These events are thus anomalous ones.

In the region of large $k_\perp$ values the perturbative language is well defined, and no problems should arise. As smaller and smaller $k_\perp$'s are considered, however, one could expect event properties that are intermediate to those of VMD. In particular, multiple parton–parton interactions could be possible, and this would affect the relation between calculated jet cross sections and the total event cross section. Previously we had to introduce a large $p_{\perp\min}^{\mathrm{anom}}$ scale to solve the problem of too large an anomalous

cross section, which means we left an unpopulated hole in the middle of Fig. 13b (indicated by a question mark). The hope is that multiple interactions would provide a natural resolution of this problem, in the sense that most anomalous events have one hard scattering above $p_{\perp\min}^{\rm anom}$, while the anomalous region with $p_\perp < p_{\perp\min}^{\rm anom}$ does not significantly contribute new events but rather further interactions inside the events above.

To study the issue, it is convenient to use the eikonal formalism. The inelastic γp cross section can then be written as (see e.g. [15])

$$\sigma_{\rm inel}^{\gamma\rm p}(s) = \sigma_{\rm dir}^{\gamma\rm p}(s) + \sum_V \frac{4\pi\alpha_{\rm em}}{f_V^2} \int {\rm d}^2b \left\{1 - \exp(-2\chi^{V\rm p}(s,b))\right\}$$
$$+ \frac{\alpha_{\rm em}}{2\pi} \sum_{\rm q} 2e_{\rm q}^2 \int_{k_0^2} \frac{{\rm d}k_\perp^2}{k_\perp^2} \int {\rm d}^2b \left\{1 - \exp(-2\chi^{a\rm p}(s,b))\right\} \ . \qquad (21)$$

Here a is used to notate an anomalous $\rm q\overline{q}$ state of the photon, characterized by the q flavour and the $k_\perp$ value. The prefactors $4\pi\alpha_{\rm em}$ and $(\alpha_{\rm em}/2\pi)\, 2e_{\rm q}^2\, {\rm d}k_\perp^2/k_\perp^2$ give the probabilities to find a given vector meson or anomalous state in the photon. The vector-meson contribution could alternatively also be written as an integral over an effective $k_\perp$ range; duality between the perturbative rate, $\gamma \to {\rm u\overline{u}}, {\rm d\overline{d}}$, and the non-perturbative one, $\gamma \to \rho^0, \omega^0$, is fulfilled if $k_{\perp\max}/k_{\perp\min} \approx 4$. For illustrative purposes we use $k_\rho \approx m_\rho/2 \approx 0.35$ GeV below as a typical $k_\perp$ scale of vector-meson production, so that a reasonable range could be from $k_{\perp\min} = 0.15$ GeV to $k_{\perp\max} = 0.6$ GeV.

The subsequent integrals over the impact parameter b space in eq. (21) give the cross section of a specific state. For simplicity, the eikonals χ are assumed to factorize:

$$2\chi^{i\rm p}(s,b) = \left[\sigma_{\rm soft}^{i\rm p}(s) + \sigma_{\rm hard}^{i\rm p}(s)\right] A^{i\rm p}(b) \qquad i = V, a \ . \qquad (22)$$

Assuming Gaussian wave functions, the overlap function $A(b)$ becomes

$$A^{i\rm p}(b) = \int {\rm d}^2b' \, \frac{e^{-b'^2/2r_i^2}}{2\pi r_i^2} \, \frac{e^{-(\mathbf{b}-\mathbf{b}')^2/2\mathbf{r}_{\rm p}^2}}{2\pi r_{\rm p}^2} = \frac{1}{2\pi(r_i^2 + r_{\rm p}^2)} \exp\left(-\frac{b^2}{2(r_i^2 + r_{\rm p}^2)}\right) \qquad i = V, a \ . \qquad (23)$$

We pick $r_{\rm p} = r_\rho = 1.2$ mb$^{1/2}$ and for anomalous states $r_a = r_\rho k_\rho/k_\perp$, i.e. a size inversely proportional to the virtuality of the state.

The $\sigma_{\rm hard}$ term in the eikonal is obtained by explicit integration of the hard scattering matrix elements above the $p_{\perp\min}$ scale, where now the same cut-off is used for the anomalous as for the VMD component. The region below $p_{\perp\min}$ is associated with the $\sigma_{\rm soft}$ term. Since perturbation theory cannot be used here, some educated guess has to be made, e.g. based on the desire to obtain a sensible total cross section at small energies, where the hard cross section is negligible. We have chosen

$$\sigma_{\rm soft}(s) = (30 \text{ mb}) \left(1 - \frac{\rm k_\perp^2}{\rm p_{\perp min}^2}\right) \theta(\rm p_{\perp min} - k_\perp) \ . \qquad (24)$$

For the VMD components, this is about 30 mb. The soft term is reduced as anomalous components of larger $k_\perp$ are considered, since the soft region is cut off from below by $p_\perp > k_\perp$ (see Fig. 13b), so that $\sigma_{\rm soft} = 0$ for $k_\perp > p_{\perp\rm min}$ in our approach.

The result is shown in Fig. 14a, as a function of $k_\perp$. Note that the effects of eikonalization decrease with increasing $k_\perp$, as the input hard cross section is reduced. By using a logarithmic scale in $k_\perp$ to take into account the basic $\mathrm{d}k_\perp^2/k_\perp^2$ probability distribution in $k_\perp$, and using a range $k_{\perp\rm max}/k_{\perp\rm min} \approx 4$ for the VMD component, the areas underneath the curves directly give the relevant total cross sections. (To obtain $\sigma^{\gamma\rm p}$, everything is to be multipled by the prefactor $(\alpha_{\rm em}/2\pi)\sum 2e_{\rm q}^2$). Since the k_0 scale in principle is a free parameter, we have continued all anomalous and direct curves to $k_0 = 0.4$ GeV, although the preferred value is more in the range 0.5–0.6 GeV. The matching of the VMD and anomalous jet cross sections for $k_\perp \approx 0.4$ GeV is a non-trivial feature, indicating that a perturbative branching $\gamma \to \mathrm{q\overline{q}}$ at this scale, when consequently evolved to the region above $p_{\perp\rm min}$, is qualitatively not so different from standard parton distributions in the pion (this is confirmed by inspection). It is thus partly related to the issue of dynamically generated parton distributions [16]. The direct cross section is also shown differentially in $k_\perp$; it should be noted that this cross section is dampened at small $k_\perp$ by the requirement that the proton structure functions vanish in the limit $Q^2 \to 0$ [1].

In GVMD approaches, it is often assumed that the eikonalized cross section vanishes as $1/k_\perp^2$. Then the integrated cross section behaves like $\int_{k_0^2} 1/k_\perp^2\, \mathrm{d}k_\perp^2/k_\perp^2 = 1/k_0^2$, i.e. is nicely convergent. Therefore, in Fig. 14b, the results are shown when multiplied by $k_\perp^2/k_\rho^2$, so that GVMD corresponds to flat curves. We see that the GVMD hypothesis does not work perfectly in our approach: at low $k_\perp$ values the fall-off is not as steep as $1/k_\perp^2$, while it is even steeper at large $k_\perp$. The convergence is therefore assured.

The results of Fig. 14 are for a c.m. energy of 200 GeV. If the energy is increased the numerics is changed, with eikonalization playing an even more important rôle in reducing the impact of the rapidly rising jet cross section on the total cross section (both in the VMD and in the anomalous sector). The qualitative features remain unchanged, however. The concept of a smooth transition between the VMD and anomalous event classes is therefore assured.

6. Summary

In this talk I have presented an ansatz for the photon wave function. This is used as the starting point for constructing a model for γp and $\gamma\gamma$ events. Essentially all free parameters are fixed by (low-energy) γp phenomenology. Since, in this Schuler–Sjöstrand model, we start out with a more detailed subdivision of the γp total cross section than has conventionally been done in the past, our $\gamma\gamma$ model also contains a richer spectrum of possible processes. We distinguish three main event classes in γp and six in $\gamma\gamma$, but most of these contain further subdivisions. The aim is that

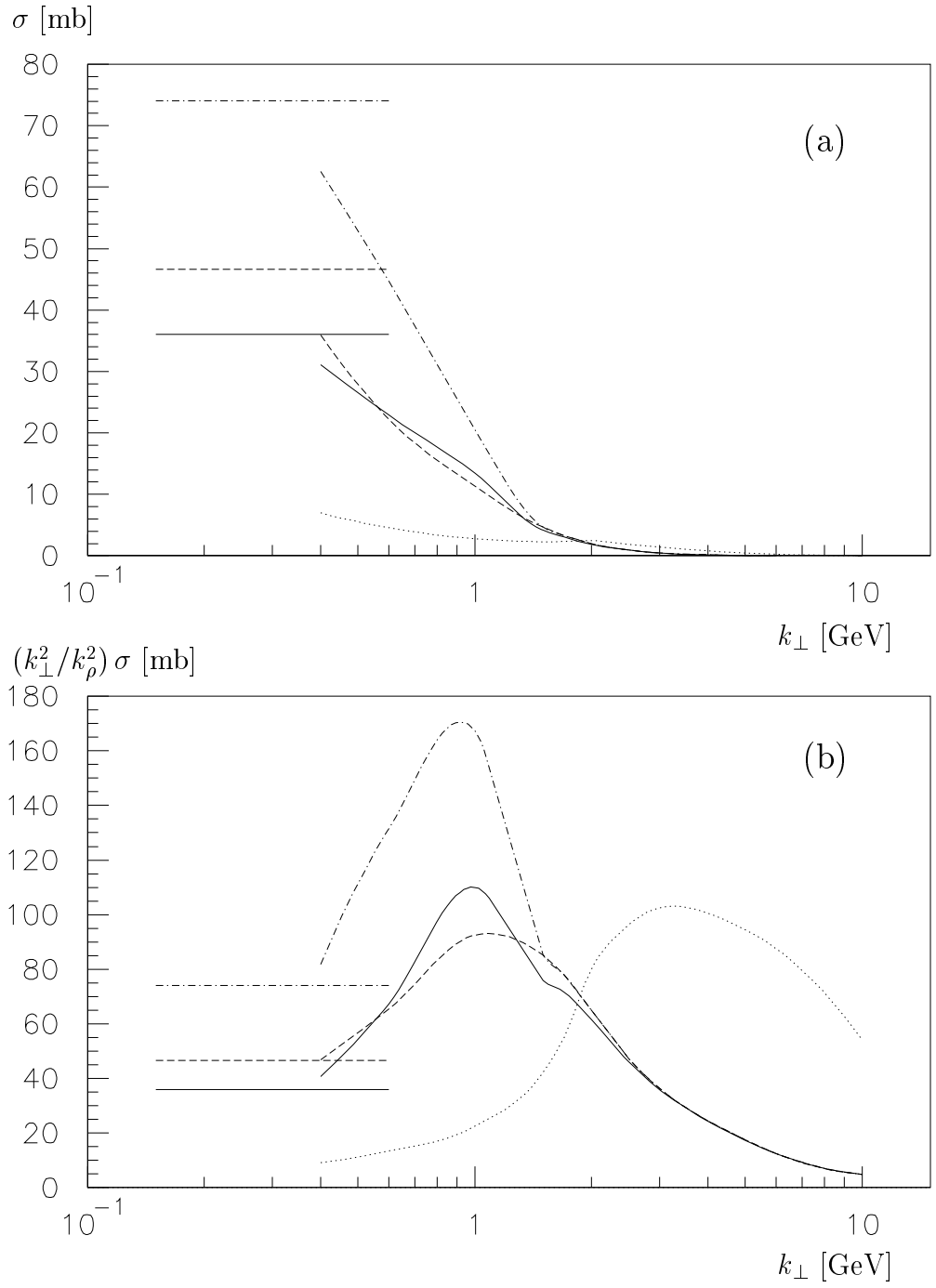

Figure 14: Cross sections as a function of the $k_\perp$ scale of the $\gamma \to q\overline{q}$ branching. Dashed curves give jet cross sections, dash-dotted jet plus soft cross sections uneikonalized, full ditto after eikonalization and dotted direct cross sections. In (b), cross sections have been multiplied by the factor $k_\perp^2/k_\rho^2$ to ease comparison with the GVMD hypothesis.

this approach should allow predictions for a broader range of observables than is addressed in conventional models. For instance, although not discussed in detail here, our approach does correlate the hard-jet physics in the central rapidity region with the structure of the beam remnants.

This does not mean that all results are complicated. We have shown that the simple Regge-theory expression $\sigma_{\mathrm{tot}}^{\gamma\gamma}(s) \approx 211\, s^{0.08} + 297\, s^{-0.45}$ [nb] comes very close to what is obtained in our full analysis. We therefore expect this expression to be good to better than 10% from a few GeV onwards, at least to the top $\gamma\gamma$ energies that could be addressed with the next generation of linear e^+e^- colliders. Also global event properties show a very simple pattern, with more activity (transverse energy, multiplicity, jets, ...) in γp events than in pp ones, and still more in $\gamma\gamma$ ones. This is perhaps contrary to the naïve image of a 'clean' point-like photon. The γp events show their intermediate status by having a photon (proton) hemisphere that looks much like $\gamma\gamma$ (pp) events, with a smooth interpolation in the middle.

Not all problems have been solved. In particular, the nature of the anomalous component of the photon is still not well understood. We have tried to sketch how a continuous transition could occur from a VMD-like to a purely perturbative state as the virtuality of the $\gamma \to q\overline{q}$ vertex is increased, but this approach is not yet fully developed. Further, we also have to devise tests that could allow us to distinguish between alternative descriptions. It should also be noted that all the discussions so far have been on incoming real photons; the transition to the deeply-inelastic-scattering region has not been addressed. Finally, more problems may well crop up once our model is compared with observations. Therefore further data from HERA, TRISTAN, LEP 1 and 2, and future linear e^+e^- colliders will have much to teach us.

Acknowledgements

I am grateful to Gerhard Schuler for having taught me a lot of what I know about the photon.

References

[1] G.A. Schuler and T. Sjöstrand, Phys. Lett. **B300** (1993) 169, Nucl. Phys. **B407** (1993) 539

[2] G.A. Schuler and T. Sjöstrand, Phys. Rev. **D49** (1994) 2257

[3] G.A. Schuler and T. Sjöstrand, CERN-TH.7193/94;
G.A. Schuler, in 'Workshop on Two-Photon Physics at LEP and HERA', eds. G. Jarlskog and L. Jönsson (Fysiska Institutionen, Lunds Universitet, Lund, 1994), p. 200

[4] Proc. 8$^{\mathrm{th}}$ Int. Workshop on Photon–Photon Collisions, Shoresh, Israel, 1988, ed. U. Karshon (World Scientific, Singapore, 1988);

Proc. 9th Int. Workshop on Photon–Photon Collisions, La Jolla, CA, USA, 1992, eds. D.O. Caldwell and H.P. Paar (World Scientific, Singapore, 1992);
Proc. Workshop on Two-Photon Physics at LEP and HERA, Lund, Sweden, 1994, eds. G. Jarlskog and L. Jönsson (Fysiska Institutionen, Lunds Universitet, Lund, 1994)

[5] C. Peterson, T.F. Walsh and P.M. Zerwas, Nucl. Phys. **B229** (1983) 301;
J.H. Field, F. Kapusta and L. Poggioli, Z. Phys. **C36** (1987) 121;
P. Aurenche et al., Nucl. Phys. **B286** (1987) 553

[6] M. Drees and R.M. Godbole, Nucl. Phys. **B339** (1990) 355, Z. Phys. **C59** (1993) 591;
J.R. Forshaw and J.K. Storrow, Phys. Rev. **D46** (1992) 4955

[7] T.H. Baur et al., Rev. Mod. Phys. **50** (1978) 261

[8] A. Donnachie and P.V. Landshoff, Phys. Lett. **B296** (1992) 227

[9] M. Froissart, Phys. Rev. **123** (1961) 1053;
A. Martin, Phys. Rev. **124** (1963) 1432

[10] ZEUS Collaboration, M. Derrick et al., Phys. Lett. **B293** (1992) 465;
H1 Collaboration, T. Ahmed et al., Phys. Lett. **B299** (1993) 374

[11] J.L. Rosner, in 'ISABELLE Physics Prospects', BNL Report 17522 (1972), p. 316

[12] T. Sjöstrand and M. van Zijl, Phys. Rev. **D36** (1987) 2019

[13] S.E. Baru et al., Z. Phys. **C53** (1992) 219, and references therein;
H.-J. Behrend et al., Z. Phys. **C51** (1991) 365

[14] T. Sjöstrand, Comput. Phys. Commun. **82** (1994) 74

[15] K. Honjo, L. Durand, R. Gandhi, H. Pi and I. Sarcevic, Phys. Rev. **D48** (1993) 1048

[16] M. Glück, E. Reya and A. Vogt, Z. Phys. **C53** (1992) 651